JURNAL BELANTARA
Deparment of Forestry
University of Mataram

Vol. 10, No.1, March (14-32)
E-ISSN 2614-3453 | P-ISSN 2614-7238
DOI: 10.29303/jbl.v10i1.1269

GEOGRAPHIC INFORMATION SYSTEM-BASED FLOOD SUSCEPTIBILITY MAPPING AT UNIVERSITAS 17 AGUSTUS 1945 SAMARINDA

Adha Bangun Chris Firdaus*, Sri Endayani, Djumansi Derita
* Department of Forestry, Faculty of Agriculture, Universitas 17 Agustus 1945, Samarinda, Indonesia
Email: abcrisfirdausa@gmail.com

ARTICLE HISTORY:
Submitted: 09, August 2026
Revised: 18, August 2026
Accepted: 21, August 2026

KEYWORDS:
DEMNAS
Field Validation
Impervious Surfaces
Rainfall
Weight Overlay

© 2027 The Authors.
Published by
The Department of Forestry,
Faculty of Agriculture,
University of Mataram.

ABSTRACT

Flooding and temporary waterlogging are recurring environmental concerns on the campus of Universitas 17 Agustus 1945 Samarinda, East Kalimantan, Indonesia, particularly in low-lying and highly impervious areas. This study aimed to map flood susceptibility within the 12.01 ha campus by integrating rainfall, slope, elevation, distance to drainage, and land use using a Geographic Information System (GIS)-based weighted overlay approach. Each parameter was classified, scored, weighted, and spatially integrated to delineate low, moderate, and high susceptibility zones. Field validation was conducted at 36 purposively selected observation points by comparing predicted susceptibility classes with observed inundation conditions. The results showed that 3.45 ha (28.7%) of the campus had low susceptibility, 5.62 ha (46.8%) moderate susceptibility, and 2.94 ha (24.5%) high susceptibility. High-susceptibility zones were concentrated in low-lying areas with gentle slopes, extensive impervious surfaces, and proximity to drainage corridors, particularly around the parking area, canteen, and student activity center. Thirty of the 36 validation points corresponded with field observations, yielding an overall agreement of 83.3%. The six mismatched points suggest that local inundation processes are not fully represented by the selected spatial parameters. These findings demonstrate that the GIS-based approach suitably identifies relative flood susceptibility and supports the prioritization of drainage improvements and environmental management interventions within the campus.

INTRODUCTION

Flooding is one of the most recurrent hydrometeorological hazards in urban areas of Indonesia, particularly in rapidly developing cities where changes in land use, increasing impervious surfaces, and limitations in drainage capacity modify natural runoff processes (Ahmed et al., 2021; Al-Bahrani et al., 2022; Aljenaid et al., 2022). Samarinda, the capital of East Kalimantan Province, is characterized by heterogeneous topography and intensive urban development, making several parts of the city susceptible to inundation during moderate to heavy rainfall (Bedair et al., 2022; Çetinkaya et al., 2022; Alqahtany, 2023). Within built-up environments, flood occurrence is not determined by rainfall alone but is also closely associated with terrain characteristics, land-use patterns, and the ability of drainage networks to convey surface runoff (Chukwuma et al., 2021; Desalegn & Mulu, 2021; Chowdhury & Hafsa, 2022). Consequently, identifying the spatial distribution of flood-susceptible areas is important for supporting land management, infrastructure planning, and environmental mitigation at the local scale (Elbeih, 2021; Dhinsa et al., 2022; Elboshy et al., 2022).

Topography plays a fundamental role in controlling the movement and accumulation of surface water (Endayani et al., 2019; El-Hadidy & Morsy, 2022; Endayani et al., 2022). Low-elevation areas and locations with gentle slopes tend to have lower gravitational drainage capacity and may therefore experience greater water accumulation (Erdem et al., 2021; Endayani et al., 2022; Endayani et al., 2023). At the same time, land-use characteristics influence infiltration and runoff generation. Built-up surfaces, roads, and parking areas generally reduce infiltration compared with vegetated and other permeable surfaces (Gürtekin & Gökçe, 2021; Ghoneim et al., 2022; Gupta et al., 2022). Drainage conditions further modify these processes because the proximity and capacity of drainage networks determine how effectively accumulated runoff can be conveyed from susceptible locations (Khalil et al., 2021; Isihak et al., 2022; Kumar et al., 2022). The interaction among these factors creates spatial variations in flood susceptibility that cannot be adequately represented by considering individual parameters independently (Larkin et al., 2021; Li et al., 2021; Li et al., 2022).

Geographic Information Systems (GIS) provide an effective framework for integrating multiple spatial variables associated with flood occurrence (Liu et al., 2021; Liu et al., 2021; Lumbreras et al., 2022). GIS-based weighted overlay techniques enable terrain, hydrological, and land-use parameters to be classified, weighted, and combined to generate spatially explicit flood-susceptibility zones. Previous studies have demonstrated the application of Geographic Information Systems (GIS) and spatial modeling for flood susceptibility and inundation mapping through integrated multi-criteria analysis and hydrodynamic modeling. In particular, GIS has been integrated with the Hydrologic Engineering Center's River Analysis System (HEC-RAS) to simulate flood inundation and identify areas potentially exposed to flooding. These studies highlight the value of integrating geospatial analysis and hydrodynamic modeling to support flood-risk assessment, spatial planning, and flood-mitigation strategies (Pepe et al., 2021; Massano et al., 2022; Murugesan et al., 2022).

Despite these developments, an important gap remains in the application of integrated flood-susceptibility assessment at a detailed local scale in Samarinda (Quan & Bansal, 2021; Stefano et al., 2021; Taloor et al., 2021). Existing GIS applications cited in the study cover a wide range of environmental and spatial-planning problems, while relatively limited attention is given to simultaneously examining the contribution of topography, land use, and drainage conditions to localized flood susceptibility and verifying the resulting spatial classification using direct field observations (Tamiru & Wagari, 2021; Turek & Stepniak, 2021; Villacreses et al., 2022). This issue is particularly relevant in highly developed environments where small differences in elevation, slope, surface cover, and drainage proximity may produce considerable differences in water accumulation (Wu et al., 2022; Xiao et al., 2022; Yousef et al., 2022). Thus, a spatial model that

integrates these environmental factors and is supported by field verification is needed to provide a more operational basis for local flood mitigation (Yudhana et al., 2021; Zhang et al., 2021; Yousef et al., 2022).

The study area provides an appropriate setting for evaluating this relationship because it contains a combination of buildings, paved roads, parking areas, open spaces, vegetation, and drainage networks. Field observations indicate that several locations experience waterlogging following moderate to heavy rainfall, particularly relatively flat areas and locations near drainage channels. The variation in built-up and permeable surfaces also provides a spatial basis for examining how land use interacts with terrain and drainage characteristics in determining flood susceptibility.

Accordingly, this study integrates rainfall, slope, elevation, distance to drainage, and land use within a GIS-based weighted overlay framework. The parameters are assigned weights of 30%, 25%, 20%, 15%, and 10%, respectively, and combined to classify the study area into low, moderate, and high flood-susceptibility zones. Unlike an assessment based solely on spatial overlay, the resulting susceptibility map is evaluated using field observations.

The dataset comprised field-observed flood inundation, Global Positioning System (GPS) coordinates, drainage conditions, DEMNAS elevation data, Sentinel-2 imagery, rainfall records, land-use data, and drainage-network data. Therefore, this study aims to integrate topographic, land-use, and drainage-related factors using a GIS-based weighted overlay approach to map flood susceptibility in Samarinda, Indonesia, and to evaluate the resulting spatial classification through field verification. Specifically, the study seeks to identify the spatial distribution of low, moderate, and high flood-susceptibility zones and determine priority locations for localized flood mitigation. The resulting information is expected to support environmentally responsive land management, drainage improvement, maintenance of permeable and vegetated surfaces, and sustainable stormwater management in urban built environments. These applications are consistent with the management implications identified from the study results.

METHOD

Study Area and Research Period

Therefore, this study aims to integrate topographic, land-use, rainfall, and drainage-related factors using a GIS-based weighted overlay approach to map flood susceptibility within the 12.01 ha campus of Universitas 17 Agustus 1945 Samarinda, East Kalimantan, Indonesia, and to evaluate the resulting spatial classification through field verification. Specifically, the study identifies the spatial distribution of low, moderate, and high flood-susceptibility zones and determines priority areas for localized flood mitigation. The findings are expected to support site-specific land management, drainage improvement, the maintenance of permeable and vegetated surfaces, and sustainable stormwater management within the university campus. The location and spatial configuration of the study area are presented in Figure 1.

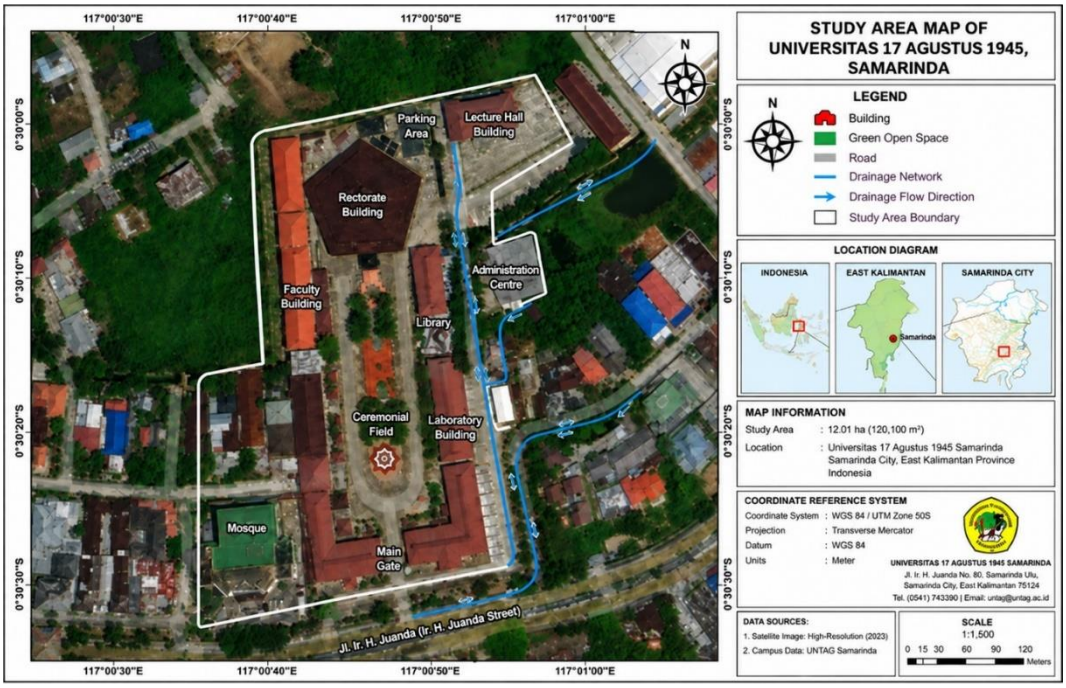


Figure 1. Geographic location and spatial extent of the study location at Universitas 17 Agustus 1945 Samarinda, East Kalimantan, Indonesia

The study location was selected because field observations indicated recurrent water accumulation at several locations, particularly in low-lying areas and locations adjacent to drainage channels. The spatial characteristics of the campus therefore provided an appropriate setting for evaluating the integration of topography, land use, rainfall, and drainage factors in GIS-based flood susceptibility mapping.

Materials, Data, and Tools

Materials, Datasets, and Pre-processing

The flood-susceptibility assessment integrated topographic, remotely sensed, hydroclimatic, drainage, land-use, and field-observation datasets. Each dataset was selected to represent a specific physical or environmental factor associated with localized surface-water accumulation. Prior to analysis, all spatial datasets were projected into a common coordinate reference system, clipped to the 12.01 ha study boundary, checked for spatial consistency, and prepared for raster-based analysis in ArcGIS. To develop a comprehensive and spatially consistent flood-susceptibility model, this study integrated multiple datasets representing the principal topographic, hydroclimatic, land-surface, drainage, and field-observation characteristics of the campus environment. The characteristics, sources, and preprocessing procedures of each dataset are described below.

a. Topographic data

Elevation information was obtained from the Indonesian National Digital Elevation Model (*Digital Elevation Model Nasional*/DEMNAS) provided by the Geospatial Information Agency of Indonesia (*Badan Informasi Geospasial*/BIG). The DEMNAS dataset, with a spatial resolution of approximately 8.1 m, was used to represent local terrain conditions. The DEM was projected to the common coordinate system and clipped to the study boundary. Elevation values were subsequently extracted directly from the DEM, whereas the slope raster was derived using the GIS slope function and expressed as percentage slope. These datasets represented the influence of terrain height and surface gradient on runoff movement and localized water accumulation.

b. Sentinel-2 imagery

Sentinel-2 Multi Spectral Instrument (MSI) Level-2A surface-reflectance imagery acquired on [INSERT EXACT ACQUISITION DATE] was used to support land-use and land-cover interpretation. The image was selected to provide the closest cloud-free representation of surface conditions during the 2026 research period. Bands B2 (Blue, 490 nm), B3 (Green, 560 nm), B4 (Red, 665 nm), and B8 (Near Infrared, 842 nm), each with a native spatial resolution of 10 m, were used for visual interpretation and discrimination of vegetation, built-up surfaces, roads, open areas, and other land-cover characteristics. Where additional discrimination of built-up surfaces and surface moisture was required, Band B11 (Short-Wave Infrared-SWIR, 1,610 nm; 20-m native resolution) was included and resampled to 10 m to provide a common working resolution. Pre-processing consisted of selecting Level-2A surface-reflectance data, screening cloud and cloud-shadow pixels, band stacking, resampling where necessary, projection to the study coordinate system, and clipping to the campus boundary.

c. Rainfall data

Rainfall observations were obtained from the Meteorology, Climatology, and Geophysics Agency of Indonesia (*Badan Meteorologi, Klimatologi dan Geofisika*/BMKG) Samarinda for [INSERT EXACT DATA PERIOD] and represented the hydroclimatic component of the flood-susceptibility model. The rainfall records were checked for completeness and consistency and subsequently aggregated according to the temporal unit adopted in the analysis. The rainfall information was transformed into the spatial representation required for GIS analysis, classified into susceptibility scores, and standardized before inclusion in the weighted-overlay model.

d. Land-use data

The campus land-use dataset was obtained from [INSERT EXACT SOURCE AND DATE] and was supplemented by Sentinel-2 interpretation and field verification. Land-use features were classified according to their hydrological surface characteristics, particularly the distinction between impervious and relatively permeable surfaces. Buildings, paved roads, parking areas, open spaces, and vegetated areas were checked and edited in the GIS environment. The resulting land-use polygons were subsequently rasterized and reclassified according to their relative contribution to surface runoff and infiltration.

e. Drainage-network data

The drainage network was obtained from [INSERT SOURCE] and verified through field observations conducted between March and July 2026. Drainage channels were represented as polyline features and checked for positional and topological consistency. The network was projected to the common coordinate system and clipped to the study boundary. A distance-to-drainage raster was then generated using GIS distance analysis. The resulting distance zones were classified and scored to represent the spatial relationship between individual locations and the existing drainage corridors.

f. Field and GPS data

Primary field observations were conducted from March to July 2026. Geographic coordinates were recorded using a GPS receiver at 36 observation locations. At each point, information on inundation occurrence, drainage condition, surrounding land use, and relevant physical characteristics was recorded. Where available, flood depth, inundated area, and inundation duration were also documented. GPS coordinates were checked for recording errors, transformed into GIS point features, and projected to the same coordinate reference system as the other datasets.

Following preprocessing, the elevation, slope, rainfall, distance-to-drainage, and land-use datasets were converted into spatially compatible thematic layers. Each layer was reclassified into standardized susceptibility scores before implementation of the weighted-overlay model. Rainfall, slope, elevation, distance to drainage, and land use were assigned weights of 30%, 25%,

20%, 15%, and 10%, respectively. The resulting flood-susceptibility map was subsequently compared with the 36 field-observation points to evaluate agreement between GIS-derived susceptibility classes and observed inundation conditions. The main equipment used during field surveys included a GPS receiver, measuring tape, mobile phone/camera, and field stationery. Spatial data processing, database preparation, raster classification, distance analysis, and weighted overlay analysis were performed using ArcGIS, while tabular data processing and descriptive calculations were performed using Microsoft Excel.

Research Design

This study employed a quantitative spatial research design using a (GIS)-based weighted overlay approach. The research consisted of five major stages: (1) collection and preprocessing of spatial and field data; (2) generation of thematic layers representing flood-conditioning factors; (3) classification and scoring of each parameter; (4) integration of the parameters using weighted overlay analysis; and (5) field validation of the resulting flood susceptibility map (Villacreses et al., 2022; Wu et al., 2022; Xiao et al., 2022). Five parameters were incorporated into the model: rainfall, slope, elevation, distance to drainage, and land use. These variables represented hydroclimatic, topographic, drainage, and surface-cover characteristics associated with the spatial occurrence of inundation within the study area. The overall methodological framework can be summarized as (Taloor et al., 2021; Tamiru & Wagari, 2021; Turek & Stepniak, 2021) (Figure 2).

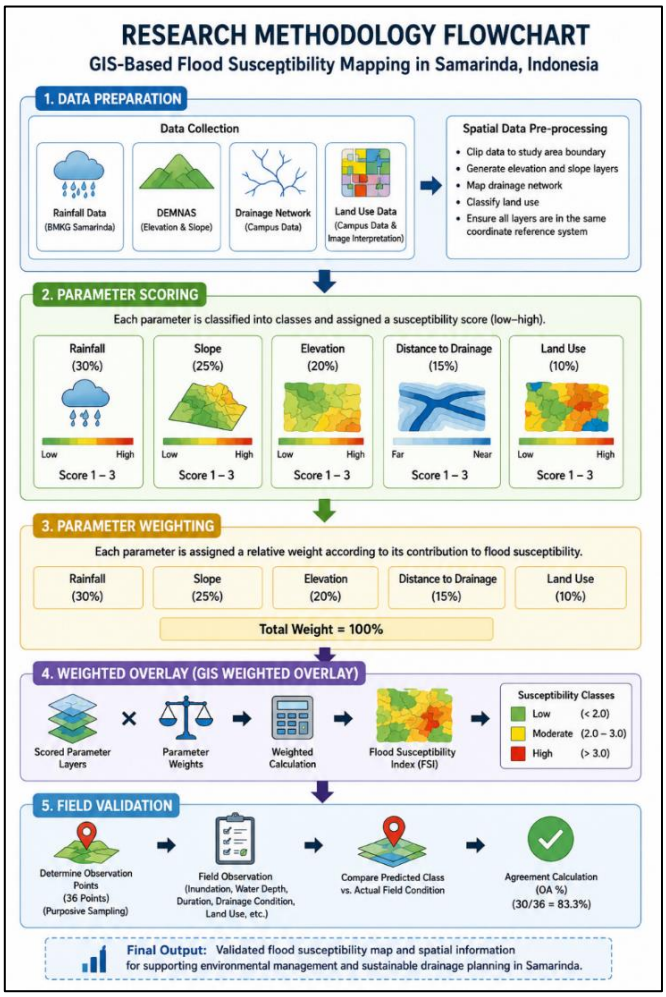


Figure 2. Methodological Framework for GIS-Based Flood Susceptibility Mapping Using Weighted Overlay and Field Validation

Preparation of Flood Susceptibility Parameters

Topographic characteristics were derived from DEMNAS. The Digital Elevation Model was clipped to the study boundary and used to generate elevation and slope layers. Lower elevations and gentler slopes were assigned higher susceptibility scores because these conditions tend to facilitate water accumulation, whereas higher elevations and steeper slopes were assigned lower scores (Ahmed et al., 2021; Al-Bahrani et al., 2022; Aljenaid et al., 2022). Land-use information was obtained from the campus land-use data and supported by interpretation of spatial imagery. Land-use classes were differentiated according to their surface characteristics. Built-up and highly impervious surfaces were considered more susceptible to surface-water accumulation than vegetated or permeable areas because of their relatively limited infiltration capacity (Bedair et al., 2022; Çetinkaya et al., 2022; Alqahtany, 2023). Drainage influence was represented by distance to drainage. The campus drainage network was spatially mapped, and distance zones were generated to represent the spatial relationship between locations and drainage corridors. This layer was subsequently classified and scored for integration into the weighted overlay model. Rainfall represented the hydroclimatic component of the model and was derived from BMKG Samarinda data. All spatial layers were prepared within a consistent spatial reference framework before overlay analysis.

Parameter Weighting and GIS-Based Weighted Overlay

Each parameter was classified and assigned a relative weight according to its contribution to flood susceptibility. Based on the weighting scheme used in the study, rainfall received the highest weight (30%), followed by slope (25%), elevation (20%), distance to drainage (15%), and land use (10%), resulting in a total weight of 100% (Table 1).

Table 1. Parameters and weights used for flood susceptibility mapping

No.	Parameter	Weight (%)
1	Rainfall	30
2	Slope	25
3	Elevation	20
4	Distance to drainage	15
5	Land use	10
	Total	**100**

Source: European Space Agency (ESA)/Copernicus Sentinel-2.

The weighted overlay model was expressed as:

$$FSI = (0.30R) + (0.25S) + (0.20E) + (0.15D) + (0.10LU)$$

Description:

FSI = the Flood Susceptibility Index,
R = the rainfall score,
S = the slope score,
E = the elevation score,
D = the distance-to-drainage score, and
LU = the land-use score.

The weighted value of each raster cell was calculated by multiplying the standardized parameter score by its corresponding weight and summing all weighted parameters. Higher FSI values represented locations with greater relative susceptibility to flooding (Taloor et al., 2021; Tamiru & Wagari, 2021; Turek & Stepniak, 2021).

Flood Susceptibility Classification

The resulting composite index was reclassified into three flood susceptibility classes: low, moderate, and high. Based on the classification thresholds used in the original study, index values below 2.0 were classified as low susceptibility, values between 2.0 and 3.0 as moderate susceptibility, and values above 3.0 as high susceptibility (Table 2) (Chowdhury & Hafsa, 2022; Chukwuma et al., 2021; Desalegn & Mulu, 2021).

Table 2. Flood susceptibility classification

FSI Score	Susceptibility Class	Interpretation
< 2.0	Low	Relatively low potential for inundation
2.0–3.0	Moderate	Moderate potential for inundation
> 3.0	High	Relatively high potential for inundation

The area of each susceptibility class was subsequently calculated in hectares and as a percentage of the total study area.

Field Observation and Sampling

Field observations were conducted to identify actual inundation conditions and to support validation of the GIS model. Observation locations were selected using purposive sampling, considering locations known to experience flooding based on preliminary field observations and information obtained from the campus community. A total of 36 observation points were used. At each point, geographic coordinates and local environmental conditions were recorded. The field assessment included observations of inundation occurrence, drainage conditions, surrounding land use, and other physical characteristics associated with water accumulation (Figure 3). For locations experiencing inundation, field information included flood depth, inundated area, and duration of inundation where these data were available. These observations provided empirical information for comparison with the susceptibility classes generated by the GIS model.

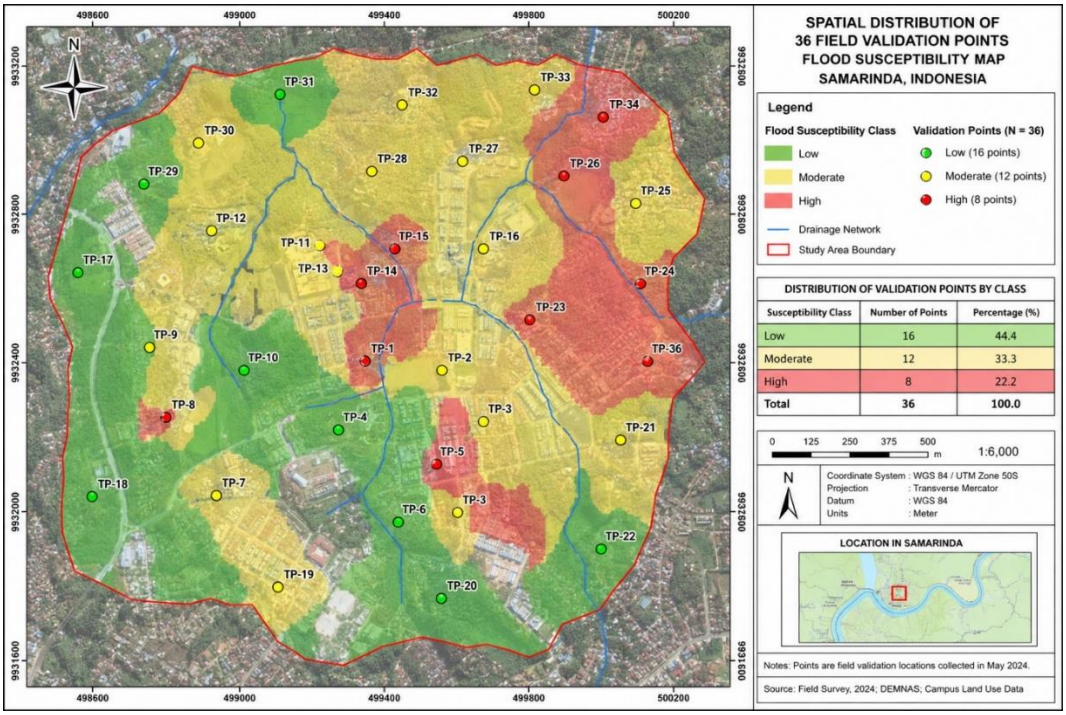


Figure 3. Spatial Distribution of Field Validation Points on the Flood Susceptibility Map

Model Validation

The flood-susceptibility map was validated using 36 purposively selected field-observation points. At each point, the GIS-derived susceptibility class (low, moderate, or high) was extracted and compared with the corresponding field condition based on observed inundation characteristics, including inundation occurrence, flood depth, inundated area, duration, drainage condition, and surrounding land use. A validation point was considered to agree with the model when the field-observed inundation condition was consistent with the susceptibility level assigned by the GIS model. Conversely, a point was classified as non-matching when the observed field condition was inconsistent with the predicted susceptibility class. Of the 36 observation points, 30 showed agreement between the GIS-derived class and field observations, whereas six points showed disagreement. Overall Agreement (OA) was therefore calculated as (Pepe et al., 2021; Quan & Bansal, 2021; Stefano et al., 2021):

$$OA = (Nc/Nt) \times 100 \quad (2)$$

$$OA = (30/36) \times 100 = 83.3\% \quad (3)$$

Description:

Nc = the number of matching observation points and
Nt = the total number of validation points. Thus:

The resulting 83.3% indicates that approximately eight out of ten field observations were consistent with the spatial susceptibility classes generated by the model. However, no predetermined categorical threshold was adopted in this study to classify an OA value as "strong," "good," or "excellent." Therefore, the 83.3% value is interpreted conservatively as a relatively high overall field agreement rather than as predictive accuracy. This distinction is important because the validation was based on a point-by-point comparison at 36 purposively selected locations rather than an independent confusion-matrix or Receiver Operating Characteristic–Area Under the Curve (ROC–AUC) assessment. The six non-matching points also indicate that localized inundation processes are not completely represented by the selected spatial parameters.

Data Analysis

Data were analyzed using spatial and descriptive quantitative approaches. Spatial analysis included DEM processing, slope derivation, land-use classification, drainage-distance analysis, raster reclassification, parameter weighting, and weighted overlay. Descriptive analysis was used to calculate the area and percentage of each flood susceptibility class and to summarize field validation results. The final spatial outputs consisted of thematic maps of elevation, slope, land use, drainage network/distance, and flood susceptibility, followed by a validated flood susceptibility map. The spatial distribution of the resulting classes was then interpreted in relation to topographic conditions, land-use characteristics, and drainage patterns to identify priority areas for flood mitigation and sustainable environmental management.

RESULT AND DISCUSSION

Integrated Interpretation of Drainage Proximity and Field Validation

The spatial relationship between drainage proximity and flood susceptibility requires careful interpretation because proximity to a drainage channel does not independently determine whether a location will experience flooding. Previous flood-susceptibility studies have commonly incorporated distance to drainage or rivers together with elevation, slope, rainfall, drainage

density, land use/land cover, and other hydro-topographic variables, indicating that drainage-related factors should be interpreted as components of an interacting system rather than as isolated controls. For example, flood-susceptibility assessments using GIS-based multi-criteria approaches have demonstrated that distance from drainage networks can contribute substantially to the spatial differentiation of flood-prone areas, particularly when combined with unfavorable terrain and runoff conditions (Endayani et al., 2019; El-Hadidy & Morsy, 2022; Endayani et al., 2022). Similar studies have shown that areas close to drainage or river networks may exhibit greater susceptibility where low elevation, gentle slopes, and runoff concentration coincide, although the relative importance of drainage proximity varies among study areas.

This interpretation is particularly relevant to the present campus-scale assessment. A drainage channel with adequate conveyance capacity, sufficient hydraulic gradient, unobstructed flow, and an effective downstream outlet can facilitate runoff removal and potentially reduce localized water accumulation. Conversely, locations adjacent to drainage corridors may remain susceptible when channel capacity is inadequate, outlets are obstructed, downstream conveyance is restricted, or surrounding terrain directs runoff toward local depressions. Recent GIS-based flood-susceptibility research similarly demonstrates that drainage-related variables interact with slope, elevation, rainfall, runoff, and land-cover characteristics in determining the spatial distribution of susceptible areas. In the Wadi Hanifah drainage basin, for example, distance to the drainage network was incorporated with slope, elevation, runoff, drainage density, and land use/land cover, while historical flood locations were used to validate the resulting susceptibility maps (Gürtekin & Gökçe, 2021; Ghoneim et al., 2022; Gupta et al., 2022). Thus, the concentration of high-susceptibility zones near several drainage corridors in the present study should not be interpreted as evidence that proximity to drainage itself causes flooding.

Instead, the weighted-overlay results indicate that drainage proximity spatially coincides with other unfavorable characteristics, particularly low elevation, gentle slopes, and impervious land cover. This interpretation is consistent with broader flood-susceptibility research showing that elevation, slope, drainage characteristics, land use/land cover, rainfall, and proximity to rivers or drainage networks collectively influence the spatial distribution of flood susceptibility. Studies using multi-source geospatial data have similarly demonstrated that flood-prone zones are more effectively identified by integrating several hydro-geomorphological and land-surface variables than by relying on a single conditioning factor. For example, flood-susceptibility mapping in the Western Ghats integrated elevation, slope, distance from drainage, drainage density, flow accumulation, rainfall, land use, and other environmental variables and achieved an AUC of approximately 0.84, supporting the usefulness of integrated multi-criteria spatial assessment (Khalil et al., 2021; Isihak et al., 2022; Kumar et al., 2022). Accordingly, the susceptibility classes generated in the present study represent spatial associations among multiple conditioning factors rather than causal hydrological relationships.

Field observations provide additional empirical support for this spatial interpretation. The canteen area (TP-5) recorded the greatest observed inundation depth of 40 cm, an inundated area of approximately 510 m^2, and a duration of about 5.0 hours, while the student activity center (TP-8) recorded an inundation depth of 38 cm, an inundated area of 490 m^2, and a duration of approximately 4.8 hours. Both locations were classified as highly susceptible. Similarly, the parking area (TP-1), which was classified as highly susceptible, recorded an inundation depth of 35 cm over approximately 450 m^2 and an inundation duration of 4.5 hours. In contrast, locations classified as having lower susceptibility generally exhibited shallower inundation and shorter durations. These observations indicate that locations identified by the GIS model as highly susceptible were generally associated with more pronounced field evidence of water accumulation.

The importance of validating GIS-derived susceptibility maps against observed flood information is also emphasized in previous studies. GIS-based flood-susceptibility assessments commonly

compare model outputs with historical flood inventories, observed flood locations, or remotely sensed inundation data to determine whether predicted susceptibility patterns correspond to actual flood occurrence. For example, flood-susceptibility modelling in the Swat River Basin used separate training and testing flood locations and obtained AUC values of 0.916 and 0.903 for success and prediction rates, respectively. Other GIS-based AHP and frequency-ratio approaches have similarly demonstrated strong correspondence between susceptibility maps and independent flood inventories, confirming the value of evidence-based validation for assessing the spatial reliability of susceptibility models.

In the present study, 30 of the 36 field observation points corresponded to the susceptibility classes generated by the GIS model, resulting in an overall agreement of 83.3%. This relatively high correspondence indicates that the mapped susceptibility pattern was generally consistent with the inundation conditions observed in the field. Nevertheless, this value should be interpreted as overall field agreement rather than predictive accuracy, because the validation procedure was based on a point-by-point comparison of susceptibility classes and field conditions rather than an independent ROC–AUC assessment. The six non-matching observations further demonstrate that localized inundation processes are not completely represented by the selected spatial parameters. Similar flood-susceptibility studies have emphasized that validation performance depends on the conditioning variables, quality and independence of the flood inventory, spatial resolution, modelling technique, and validation method employed.

Taken together, the spatial and field evidence indicates that the highest flood susceptibility within the campus occurs where several unfavorable characteristics overlap rather than as a consequence of drainage proximity alone. Rainfall provides the hydroclimatic input, whereas terrain configuration, impervious surface cover, and drainage conditions influence the redistribution, conveyance, and localized accumulation of runoff. The GIS-based weighted-overlay model should therefore be interpreted as a spatial screening and prioritization tool for identifying relatively susceptible locations rather than as a process-based representation of flood causality. Establishing causal hydrological relationships would require additional information on rainfall intensity and duration, drainage dimensions and conveyance capacity, runoff coefficients, flow direction and discharge, downstream boundary conditions, and preferably hydrological or hydrodynamic modelling.

Spatial Distribution of Flood Susceptibility

The weighted overlay analysis classified the 12.01 ha study area into three flood susceptibility classes: low, moderate, and high. The moderate susceptibility class occupied the largest area, covering 5.62 ha or 46.8% of the study area. Low susceptibility accounted for 3.45 ha (28.7%), whereas 2.94 ha (24.5%) was classified as highly susceptible (Table 3).

Table 3. Spatial distribution of flood susceptibility classes

Susceptibility class	Area (ha)	Percentage (%)
Low	3.45	28.7
Moderate	5.62	46.8
High	2.94	24.5
Total	**12.01**	**100.0**

Source: Authors' field survey and flood-inundation observations, 2026.

The predominance of the moderate class indicates that almost half of the study area is characterized by environmental conditions that can potentially facilitate inundation. More importantly, when the moderate and high classes are considered together, they represent 71.3% (8.56 ha) of the study area. This does not imply that 71.3% of the area will necessarily experience flooding during every rainfall event; rather, it indicates that a substantial proportion of the study

area possesses combinations of the mapped factors associated with moderate or high flood susceptibility.

The high-susceptibility zones were concentrated around the parking area, canteen, student activity center, and low-lying areas adjacent to drainage corridors. The spatial concentration of high susceptibility in these locations is consistent with the integration of topographic and land-use characteristics represented in the model. Parking and other intensively paved areas provide less permeable surfaces, while low-lying areas favor the accumulation of surface water.

This pattern highlights the importance of considering the interaction between built surfaces and local topography in small urban catchments. Rather than being uniformly distributed, flood susceptibility was concentrated in specific locations where unfavorable topographic conditions coincided with intensive land use and drainage-related constraints (Elbeih, 2021; Dhinsa et al., 2022; Elboshy et al., 2022).

Field Characteristics of Flood-Prone Locations

Field observations provided additional information regarding the physical characteristics of inundation at selected locations. Among the observation sites presented in the dataset, the canteen area (TP-5) recorded the greatest flood depth at 40 cm, an inundated area of 510 m^2, and an inundation duration of approximately 5.0 hours. The student activity center (TP-8) recorded a depth of 38 cm, an inundated area of 490 m^2, and a duration of 4.8 hours. Both locations were categorized as highly susceptible (Table 4).

Table 4. Field characteristics of selected flood observation points

Observation point	Location	Flood depth (cm)	Inundated area (m^2)	Duration (hours)	Susceptibility
TP-1	Parking area	35	450	4.5	High
TP-2	Rectorate Building	28	320	3.0	Moderate
TP-3	Forestry Faculty	22	250	2.5	Moderate
TP-4	Main campus road	18	180	2.0	Low
TP-5	Canteen area	40	510	5.0	High
TP-6	Open field	15	150	1.5	Low
TP-7	Library area	30	370	3.5	Moderate
TP-8	Student activity center	38	490	4.8	High
TP-9	Administration Office	24	280	2.8	Moderate
TP-10	Campus entrance gate	20	210	2.2	Low

Source: Authors' field survey and flood-inundation observations, 2026.

Moderate susceptibility was observed around the Rectorate Building, Forestry Faculty, Library, and Administration Office. Flood depths at these locations ranged from 22 to 30 cm, while inundation duration ranged from approximately 2.5 to 3.5 hours. In comparison, locations categorized as having lower susceptibility generally recorded shallower and shorter-duration inundation.

These field measurements support the spatial interpretation of the susceptibility map because locations categorized as highly susceptible were also characterized by relatively greater flood depth, inundated area, and duration. Nevertheless, these measurements should be interpreted as field evidence associated with the observed conditions rather than as proof of a causal

relationship between individual spatial parameters and flooding. The weighted overlay approach identifies spatial association and relative susceptibility but does not independently establish causal effects (Chukwuma et al., 2021; Desalegn & Mulu, 2021; Chowdhury & Hafsa, 2022).

Validation of the Flood Susceptibility Map

An important component of the study was the comparison between GIS-derived susceptibility classes and field observations. A total of 36 field observation points were used for verification. Of these, 30 points corresponded to the susceptibility classes predicted by the GIS model, resulting in an overall agreement of 83.3%.

The overall agreement of 83.3% obtained in this study indicates a reasonably strong correspondence between the GIS-derived susceptibility classes and the observed field conditions. This level of agreement is broadly comparable with results reported in previous flood-susceptibility studies, although direct numerical comparison should be made cautiously because different validation procedures and performance metrics were employed. For example, a GIS-based comparison of Frequency Ratio (FR) and Statistical Index (SI) models in the Upper Krishna Basin reported prediction AUC values of approximately 68.0% and 83.23%, respectively, with the SI model showing performance similar in magnitude to the 83.3% agreement obtained in the present study. In Kakegawa, Japan, GIS-based AHP and FR models were evaluated using independent training and validation flood inventories and ROC–AUC analysis; the AHP model achieved a prediction AUC of 85.5%, whereas the FR model reached 67.0%. Higher predictive performance has also been reported for more data-intensive approaches. A bivariate statistical flood-susceptibility model in the Swat River Basin achieved success and prediction AUC values of 0.916 and 0.903, respectively, using separate training and testing flood locations. Similarly, ensemble Evidential Belief Function–Support Vector Machine (EBF–SVM) modelling produced prediction rates of up to 92.11%, exceeding those of several individual models.

These differences should not be interpreted as evidence that the present model is necessarily less reliable because the performance measures are not directly equivalent. The present study used a straightforward point-by-point comparison between three GIS-derived susceptibility classes and field observations at 36 purposively selected locations, whereas many previous studies used larger historical flood inventories, independent training and testing subsets, and Receiver Operating Characteristic–Area Under the Curve (ROC–AUC) analysis to evaluate discriminatory or predictive performance. Accordingly, the 83.3% value represents overall field agreement rather than an AUC-based predictive accuracy. Nevertheless, the relatively high correspondence obtained from direct field verification suggests that the weighted-overlay model provides useful local-scale spatial screening of flood susceptibility. Future studies could strengthen this validation by increasing the number and spatial independence of validation points and by applying a confusion matrix, class-specific accuracy measures, and ROC–AUC analysis using an independent flood inventory (Bedair et al., 2022; Çetinkaya et al., 2022; Alqahtany, 2023).

However, the remaining six observation points did not correspond to the predicted classes. These discrepancies indicate that the current model does not capture all processes responsible for local inundation. The manuscript itself identifies the need for more detailed hydrological and drainage information in future studies. Therefore, the 83.3% value is more appropriately reported as overall agreement rather than comprehensive model accuracy unless a complete validation procedure, confusion matrix, and class-specific accuracy statistics are provided.

Integrated Influence of Topography, Land Use, and Drainage

The spatial and field results collectively demonstrate that areas with higher flood susceptibility were characterized by overlapping physical and land-surface constraints. Low elevation and

gentle slopes were associated with reduced surface-water conveyance, while paved land uses reduced opportunities for infiltration. Where these conditions occurred around low-lying drainage corridors, localized inundation was more evident (Ahmed et al., 2021; Al-Bahrani et al., 2022; Aljenaid et al., 2022).

The relationship between land use and susceptibility is particularly relevant to environmental management. Built-up surfaces, roads, and parking areas represent important components of the campus landscape, but increasing impermeable coverage can alter the distribution of surface runoff. The observed high susceptibility around the parking area and other intensively used locations therefore indicates the importance of maintaining an appropriate balance between built surfaces and permeable or vegetated areas.

Drainage should similarly be interpreted in conjunction with topography and land use rather than independently. The presence of drainage infrastructure alone does not guarantee low susceptibility. Field observations reported suboptimal drainage conditions and temporary stagnation before water reached the main drainage channel. Thus, drainage performance, surface elevation, and surrounding land cover need to be considered simultaneously when prioritizing mitigation.

The results consequently support an integrated approach to flood susceptibility assessment. The GIS model does not demonstrate that any individual factor causes flooding; instead, it identifies locations where multiple spatial characteristics coincide to produce relatively higher susceptibility. This distinction is important because the present study employed weighted spatial overlay rather than regression, hydrodynamic simulation, or causal analysis.

Implications for Sustainable Environmental Management

The resulting susceptibility map provides a spatial basis for prioritizing flood mitigation within the study area. Areas classified as highly susceptible, particularly the parking area, canteen, student activity center, and low-lying drainage corridors, should receive greater attention in environmental and infrastructure planning (Figure 4).

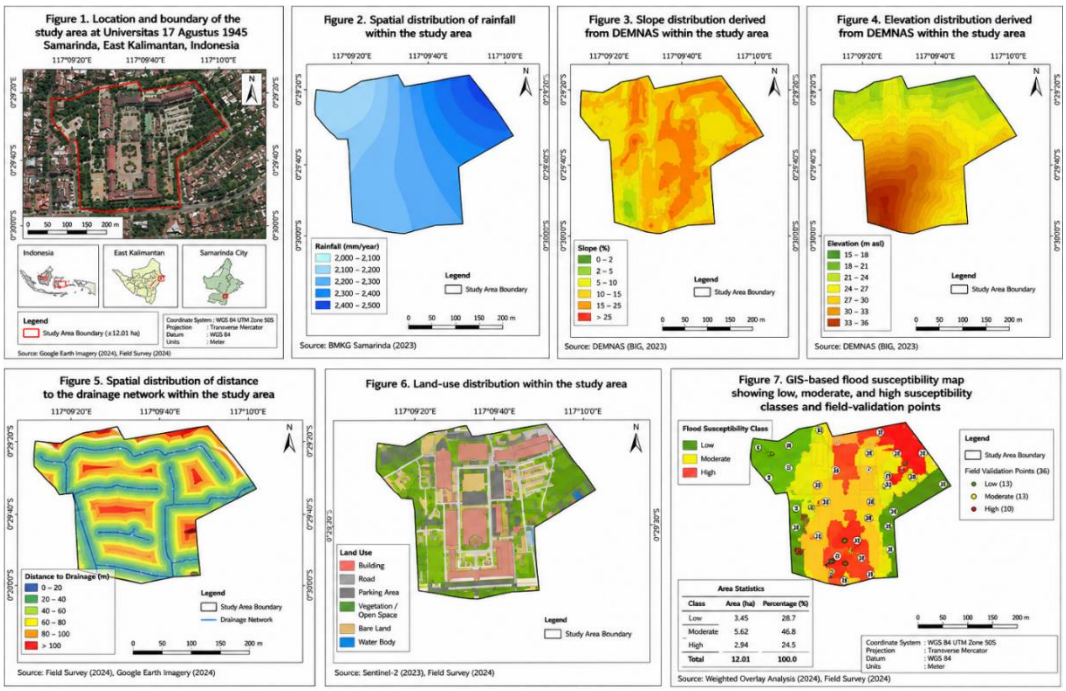


Figure 4. GIS-Based Flood Susceptibility Mapping Framework Synthesizing Topography, Land Use, and Drainage

Mitigation measures should primarily focus on improving drainage performance and maintaining water conveyance pathways, while preserving and increasing permeable and vegetated surfaces where feasible. Sustainable stormwater management should also be incorporated into future land-use planning so that additional development does not further increase surface impermeability in already susceptible locations. These recommendations are consistent with the environmental-management implications identified in the study (Lumbreras et al., 2022; Massano et al., 2022; Murugesan et al., 2022).

From a broader perspective, the principal contribution of this study is the integration of topographic, land-use, rainfall, and drainage-related spatial information with field verification at a detailed local scale. The approach provides a relatively straightforward framework for identifying priority locations where flood mitigation measures can be directed. The moderate and high susceptibility zones covering 71.3% of the study area indicate that flood-sensitive considerations should become an integral component of future spatial and environmental management.

CONCLUSION AND RECOMMENDATION

This study integrated topographic, land-use, rainfall, and drainage-related factors within a GIS-based weighted overlay framework to map flood susceptibility across the 12.01 ha campus of Universitas 17 Agustus 1945 Samarinda. The results classified 3.45 ha (28.7%) as low, 5.62 ha (46.8%) as moderate, and 2.94 ha (24.5%) as high susceptibility, with the moderate and high classes collectively covering 8.56 ha (71.3%) of the study area. High-susceptibility zones were concentrated around the parking area, canteen, student activity center, and low-lying locations adjacent to drainage corridors, where low elevation, gentle slopes, impervious surfaces, and drainage-related constraints spatially coincided. Field validation showed that 30 of 36 observation points corresponded with the GIS-derived susceptibility classes, yielding an overall agreement of 83.3%, although this value should be interpreted as spatial agreement rather than comprehensive predictive accuracy. The findings demonstrate that the weighted overlay approach provides a useful spatial screening and decision-support tool for identifying priority locations for flood mitigation, but it represents relative susceptibility rather than the probability, magnitude, or causal mechanisms of flooding and does not explicitly account for drainage capacity, temporal rainfall intensity, runoff dynamics, or hydrodynamic processes. Accordingly, mitigation should prioritize high-susceptibility locations through regular drainage maintenance, improvement of local water-conveyance capacity, preservation and expansion of permeable and vegetated surfaces, and integration of sustainable stormwater management into future campus land-use planning. Future research should incorporate more detailed rainfall, runoff, drainage-capacity, and hydrological or hydrodynamic data and employ more comprehensive validation procedures, including confusion matrices and class-specific accuracy metrics, to improve model robustness and its application to local flood-risk management.

REFERENCES

Ahmed, H. G. I., Mohamed, M. H., & Saleh, S. S. (2021). A GIS model for exploring the water pumped storage locations using remote sensing data. *Egyptian Journal of Remote Sensing and Space Science*, 24(3), 515–523. https://doi.org/10.1016/j.ejrs.2021.09.006

Al-Bahrani, H. S., Al-Rammahi, A. H., Al-Mamoori, S. K., Al-Maliki, L. A., & AL-Ansari, N. (2022). Groundwater detection and classification using remote sensing and GIS in Najaf, Iraq. *Groundwater for Sustainable Development*, 19, Article 100838. https://doi.org/10.1016/j.gsd.2022.100838

Aljenaid, S., Abido, M., Redha, G. K., AlKhuzaei, M., Marsan, Y., Khamis, A. Q., Naser, H., AlRumaidh, M., & Alsabbagh, M. (2022). Assessing the spatiotemporal changes, associated carbon stock, and potential emissions of mangroves in Bahrain using GIS and remote sensing data. *Regional Studies in Marine Science*, 52, Article 102282. https://doi.org/10.1016/j.rsma.2022.102282

Alqahtany, A. (2023). GIS-based assessment of land use for predicting increase in settlements in Al Ahsa Metropolitan Area, Saudi Arabia for the year 2032. *Alexandria Engineering Journal*, 62, 269–277. https://doi.org/10.1016/j.aej.2022.07.020

Bedair, S., Sayed, S. A., & AlMetwaly, W. M. (2022). Enhancing Hybrid Learning using Open Source GIS-Based Maps Archiving System. *Egyptian Journal of Remote Sensing and Space Science*, 25(3), 779–793. https://doi.org/10.1016/j.ejrs.2022.07.003

Çetinkaya, C., Erbaş, M., Kabak, M., & Özceylan, E. (2022). A mass vaccination site selection problem: An application of GIS and entropy-based MAUT approach. *Socio-Economic Planning Sciences,* 85, Article 101376. https://doi.org/10.1016/j.seps.2022.101376

Chowdhury, M. S., & Hafsa, B. (2022). Multi-decadal land cover change analysis over Sundarbans Mangrove Forest of Bangladesh: A GIS and remote sensing-based approach. *Global Ecology and Conservation*, 37, Article e02151. https://doi.org/10.1016/j.gecco.2022.e02151

Chukwuma, E. C., Okonkwo, C. C., Ojediran, J. O., Anizoba, D. C., Ubah, J. I., & Nwachukwu, C. P. (2021). A Gis Based Flood Vulnerability Modelling Of Anambra State Using An Integrated IVFRN-DEMATEL-ANP Model. *Heliyon*, *7*(9), Article e08048. https://doi.org/10.1016/j.heliyon.2021.e08048

Desalegn, H., & Mulu, A. (2021). Mapping flood inundation areas using GIS and HEC-RAS model at Fetam River, Upper Abbay Basin, Ethiopia. *Scientific African*, 12, Article e00834. https://doi.org/10.1016/j.sciaf.2021.e00834

Dhinsa, D., Tamiru, F., & Tadesa, B. (2022). Groundwater potential zonation using VES and GIS techniques: A case study of Weserbi Guto catchment in Sululta, Oromia, Ethiopia. *Heliyon*, 8(8), Article e10245. https://doi.org/10.1016/j.heliyon.2022.e10245

El-Hadidy, S. M., & Morsy, S. M. (2022). Expected spatio-temporal variation of groundwater deficit by integrating groundwater modeling, remote sensing, and GIS techniques. *Egyptian Journal of Remote Sensing and Space Science*, 25(1), 97–111. https://doi.org/10.1016/j.ejrs.2022.01.001

Elbeih, S. F. (2021). Evaluation of agricultural expansion areas in the Egyptian deserts: A review using remote sensing and GIS. In *Egyptian Journal of Remote Sensing and Space Science*, 24(3P2), 889–906. https://doi.org/10.1016/j.ejrs.2021.10.004

Elboshy, B., Alwetaishi, M., M. H. Aly, R., & Zalhaf, A. S. (2022). A suitability mapping for the PV solar farms in Egypt based on GIS-AHP to optimize multi-criteria feasibility. *Ain Shams Engineering Journal*, 13(3), Article 101618. https://doi.org/10.1016/j.asej.2021.10.013

Endayani, S., Sadono, R., Kusumandari, A., & Hartono. (2019). Social and economic vulnerability in the sub-watershed of Karang Mumus, East Kalimantan Province. *Jurnal Manajemen Hutan Tropika*, 25(2), 93–103. https://doi.org/10.7226/jtfm.25.2.93

Endayani, S., Sadono, R., Kusumandari, A., Hartono, & Baiquni, M. (2022). Horizontal and Vertical Geometric Accuracy of Agisoft Photoscan and Pix4D Mapper Software at Kebun Raya Universitas Mulawarman in Samarinda, East Kalimantan, Indonesia. *International Journal*

on Advanced Science, Engineering and Information Technology, 12(5), 2132–2139. https://doi.org/10.18517/ijaseit.12.5.16362

Endayani, S., Stefano, A., Fathiah, Hamka, & Lisnawati, A. (2023). Forest Land Change Assessment of Karang Mumus Sub-Watershed Area. *Jurnal Manajemen Hutan Tropika*, 29(1), 35–44. https://doi.org/10.7226/jtfm.29.1.35

Endayani, S., Stefano, A., Fathiah, Purbawati, & Rosanti, I. (2022). Monitoring Forest Area Change Using Quickbird. *Biotropia*, 29(2), 161–170. https://doi.org/10.11598/btb.2022.29.2.1690

Erdem, F., Atun, R., Yigit Avdan, Z., Atila, I., & Avdan, U. (2021). Drought analysis of Van Lake Basin with remote sensing and GIS technologies. *Egyptian Journal of Remote Sensing and Space Science*, 24(3), 1093–1102. https://doi.org/10.1016/j.ejrs.2021.10.006

Ghoneim, S. M., Yehia, M. A., Salem, S. M., & Ali, H. F. (2022). Integrating remote sensing data, GIS analysis and field studies for mapping alteration zones at Wadi Saqia area, central Eastern Desert, Egypt. *Egyptian Journal of Remote Sensing and Space Science*, 25(1), 323–336. https://doi.org/10.1016/j.ejrs.2022.02.001

Gupta, L., Agrawal, N., Dixit, J., & Dutta, S. (2022). A GIS-based assessment of active tectonics from morphometric parameters and geomorphic indices of the Assam Region, India. *Journal of Asian Earth Sciences: X*, 8, Article 100115. https://doi.org/10.1016/j.jaesx.2022.100115

Gürtekin, E., & Gökçe, O. (2021). Estimation of erosion risk of Harebakayiş sub-watershed, Elazig, Turkey, using GIS-based RUSLE model. *Environmental Challenges*, 5, Article 100315. https://doi.org/10.1016/j.envc.2021.100315

Isihak, S., Akpan, U., & Bhattacharyya, S. (2022). Evolution of GIS-based rural electrification planning models and an application of OnSSET in Nigeria. *Renewable and Sustainable Energy Transition*, *2*, Article 100019. https://doi.org/10.1016/j.rset.2022.100019

Khalil, N., Mhanna, M., & Assaf, E. H. (2021). Horizontal corridor optimization of highway using GIS & CFSC method in mountainous areas. *Egyptian Journal of Remote Sensing and Space Science*, 24(3), 509–514. https://doi.org/10.1016/j.ejrs.2021.08.008

Kumar, M., Singh, P., & Singh, P. (2022). Integrating GIS and remote sensing for delineation of groundwater potential zones in Bundelkhand Region, India. *Egyptian Journal of Remote Sensing and Space Science*, 25(2), 387–404. https://doi.org/10.1016/j.ejrs.2022.03.003

Larkin, A., Gu, X., Chen, L., & Hystad, P. (2021). Predicting perceptions of the built environment using GIS, satellite, and street view image approaches. *Landscape and Urban Planning*, 216, Article 104257. https://doi.org/10.1016/j.landurbplan.2021.104257

Li, S., Zhang, M., Yuan, F., Li, X., Wang, C., Long, J., & Jiao, J. (2022). Isotope spatiotemporal analysis and prospecting indication based on GIS in Tibet. *Ore Geology Reviews*, 147, Article 104997. https://doi.org/10.1016/j.oregeorev.2022.104997

Li, W., Winter, P. L., Milburn, L. A., & Padgett, P. E. (2021). A dual-method approach toward measuring the built environment: sampling optimization, validity, and efficiency of using GIS and virtual auditing. *Health and Place*, 67, Article 102482. https://doi.org/10.1016/j.healthplace.2020.102482

Liu, H., Zhang, Z., Chen, T., Yang, J., Li, Q., & He, D. (2021). Simplified Modelling of Transient Ground Potential Rise of GIS in Ultra-high-voltage Substations with Hybrid Reactive Power Compensation. *Electric Power Systems Research*, 199, Article 107441. https://doi.org/10.1016/j.epsr.2021.107441

Liu, Q., Zhai, G., & Lu, X. (2021). Integrated land-sea surveying and mapping of intertidal zone based on high-definition remote sensing images and GIS technology. *Microprocessors and Microsystems*, 82, Article 103937. https://doi.org/10.1016/j.micpro.2021.103937

Lumbreras, M., Diarce, G., Martin-Escudero, K., Campos-Celador, A., & Larrinaga, P. (2022). Design of district heating networks in built environments using GIS: A case study in Vitoria-Gasteiz, Spain. *Journal of Cleaner Production*, 349, Article 131491. https://doi.org/10.1016/j.jclepro.2022.131491

Massano, M., Macii, E., Lanzini, A., Patti, E., & Bottaccioli, L. (2022). A GIS Open-Data Co-Simulation Platform for Photovoltaic Integration in Residential Urban Areas. *Engineering*, 26, 198-213. https://doi.org/10.1016/j.eng.2022.06.020

Murugesan, M., Venkatesan, P., Kumar, S., Thangavelu, P., Rose, W., John, J., Castro, M., Manivannan, T., Mohan, V. R., & Rupali, P. (2022). Epidemiological investigation of the COVID-19 outbreak in Vellore district in South India using Geographic Information Surveillance (GIS). *International Journal of Infectious Diseases*, 122, 669–675. https://doi.org/10.1016/j.ijid.2022.07.010

Pepe, M., Costantino, D., Alfio, V. S., Restuccia, A. G., & Papalino, N. M. (2021). Scan to BIM for the digital management and representation in a 3D GIS environment of a cultural heritage site. *Journal of Cultural Heritage*, 50, 115–125. https://doi.org/10.1016/j.culher.2021.05.006

Quan, S. J., & Bansal, P. (2021). A systematic review of GIS-based local climate zone mapping studies. In *Building and Environment*, 196, Article 107791. https://doi.org/10.1016/j.buildenv.2021.107791

Stefano, A., Endayani, S., & Sadono, R. (2021). Combining the Traditional and Modern Architecture in Taman Samarendah Plan, Samarinda City, East Kalimantan Province, Indonesia. *International Journal on Advanced Science, Engineering and Information Technology*, 11(2), 705–711. https://doi.org/10.18517/ijaseit.11.2.8341

Taloor, A. K., Adimalla, N., & Goswami, A. (2021). Remote Sensing and GIS applications in Geoscience. *Applied Computing and Geosciences*, 11, Article 100065. https://doi.org/10.1016/j.acags.2021.100065

Tamiru, H., & Wagari, M. (2021). Evaluation of data-driven model and GIS technique performance for identification of Groundwater Potential Zones: A case of Fincha Catchment, Abay Basin, Ethiopia. *Journal of Hydrology: Regional Studies*, 37, Article 100902. https://doi.org/10.1016/j.ejrh.2021.100902

Turek, T., & Stepniak, C. (2021). Areas of integration of GIS technology and smart city tools. Research findings. *Procedia Computer Science*, 192, 4681–4690. https://doi.org/10.1016/j.procs.2021.09.246

Villacreses, G., Martínez-Gómez, J., Jijón, D., & Cordovez, M. (2022). Geolocation of photovoltaic farms using Geographic Information Systems (GIS) with Multiple-criteria decision-making (MCDM) methods: Case of the Ecuadorian energy regulation. In *Energy Reports*, 8, 3526–3548. https://doi.org/10.1016/j.egyr.2022.02.152

Wu, X., Xu, C., Xu, X., Chen, G., Zhu, A., Zhang, L., Yu, G., & Du, K. (2022). A Web-GIS hazard information system of the 2008 Wenchuan Earthquake in China. *Natural Hazards Research*, 2(3), 210-217. https://doi.org/10.1016/j.nhres.2022.03.003

Xiao, Y., Yan, Y., Yu, Y. S., Wang, B., & Liang, Y. H. (2022). Research on pose adaptive correction method of indoor rail-mounted inspection robot in GIS Substation. *Energy Reports*, 8, 696–705. https://doi.org/10.1016/j.egyr.2022.03.155

Yousef, G. A., Elazony, M. A., Abdelsattar, A., Sewailam, M. M., & Elsaid, O. H. (2022). Applying an integrated Remote Sensing-GIS approach in the documentation of handicraft centers at New Valley Governorate, Egypt. *Egyptian Journal of Remote Sensing and Space Science*, 25(3), 731–739. https://doi.org/10.1016/j.ejrs.2022.04.004

Yudhana, A., Sulistyo, D., & Mufandi, I. (2021). GIS-based and Naïve Bayes for nitrogen soil mapping in Lendah, Indonesia. *Sensing and Bio-Sensing Research*, 33, Article 100435. https://doi.org/10.1016/j.sbsr.2021.100435

Zhang, S., Liu, X., Li, R., Wang, X., Cheng, J., Yang, Q., & Kong, H. (2021). AHP-GIS and MaxEnt for delineation of potential distribution of Arabica coffee plantation under future climate in Yunnan, China. *Ecological Indicators*, 132, Article s108339. https://doi.org/10.1016/j.ecolind.2021.108339